Giant exciton-enhanced shift currents and direct current conduction with subbandgap photo excitations produced by many-electron interactions

Yang-Hao Chan[a,b,c], Diana Y. Qiu[a,b], Felipe H. da Jornada[a,b], and Steven G. Louie[a,b,1]

[a]Department of Physics, University of California, Berkeley, CA 94720-7300; [b]Materials Sciences Division, Lawrence Berkeley National Laboratory, Berkeley, CA 94720; and [c]Institute of Atomic and Molecular Sciences, Academia Sinica, 10617 Taipei, Taiwan

Edited by Naoto Nagaosa, Rikagaku Kenkyujo Sohatsu Bussei Kagaku Kenkyu Center, Saitama, Japan, and approved May 15, 2021 (received for review April 24, 2019)

Shift current is a direct current generated from nonlinear light–matter interaction in a noncentrosymmetric crystal and is considered a promising candidate for next-generation photovoltaic devices. The mechanism for shift currents in real materials is, however, still not well understood, especially if electron–hole interactions are included. Here, we employ a first-principles interacting Green's-function approach on the Keldysh contour with real-time propagation to study photocurrents generated by nonlinear optical processes under continuous wave illumination in real materials. We demonstrate a strong direct current shift current at subbandgap excitation frequencies in monolayer GeS due to strongly bound excitons, as well as a giant excitonic enhancement in the shift current coefficients at above bandgap photon frequencies. Our results suggest that atomically thin two-dimensional materials may be promising building blocks for next-generation shift current devices.

shift current | excitonic effects | first principles | time-dependent GW

When continuous wave light is shone on a noncentrosymmetric crystal, a direct current (DC) can arise due to a second-order optical response of the crystal. The origin of this current is interpreted to be related to the "shift" (1–4) of the intracell coordinates of the excited electron. This so-called shift current is proposed as an alternative to the photocurrent generated by traditional semiconductor p–n junctions (i.e., a junction between hole-doped [p-type] and electron-doped [n-type] semiconductors) for photovoltaic applications (5, 6). Unlike conventional photovoltaic devices, shift current is a bulk phenomenon, which does not require a p–n junction to separate the optically generated electron–hole pair for a DC. Moreover, recent studies reveal that the photocarriers in shift current can have long travel distances, which is distinct from the usual drift transport mechanism in traditional solar cells (7, 8) and makes shift current a promising candidate for efficient energy conversion.

Despite many investigations over the past decade, a basic understanding of shift currents is far from complete. Most theoretical studies to date rely on the assumption of having noninteracting particles (3–6, 9–11). Given that it is well known that light-induced electron–hole pairs can form bound or resonant excitons (correlated electron–hole states), which dominate and qualitatively change the absorption features of semiconductors, electron–hole interactions or excitons are expected to play a large role in shift currents, especially for reduced dimensional systems. However, it is not straight forward to generalize existing ab initio methods [such as the ab initio GW plus Bethe-Salpeter equation (GW-BSE) approach (12)], used to understand and compute excitonic effects in linear optical absorption, to study nonlinear optical responses. Different model approaches to investigate the effects of many-electron interactions on nonlinear optical responses of materials have been proposed. For instance, a Floquet-based model Hamiltonian formalism showed that excitonic effects enhance nonlinear response (13). In the specific case of second harmonic generation, first-principles approaches have been developed and applied to real materials, for instance, by making an approximation to the full many-body perturbation theory treatment (14, 15) or to the time-dependent density function theory, in which electron interaction effects are taken into account via simplified kernels (16). A real-time formulation based on propagating the time-dependent Schrodinger equation has also been developed (17) and applied to second harmonic generation (18). For shift currents in real materials, only one recent study considered the effects of excitons on the linear optical coefficient that might influence shift currents, but these authors included only the effects of excitons on the electromagnetic field profile in a bulk sample, and the crucial process of shift current generation itself is still treated within an independent-particle picture (11). Thus, there is still no first-principles calculation and understanding of the role of many-electron interactions, particularly those due to excitons, on shift currents.

Here, we show from first principles that 1) bound exciton states in the band gap can generate substantial shift currents, and 2) excitonic effects in the electron–hole continuum part of the spectrum can also greatly enhance shift currents due to the enhancement of the optical matrix elements from the coherence of the electron–hole pairs and to interexciton couplings that arose in the nonlinear responses.

Methods

To carry out the calculation of shift currents including many-electron interactions and therefore excitonic effects, we employ an ab initio approach to study in general nonlinear optical phenomena in real materials based on real-time propagation of the nonequilibrium interacting Green's function

Significance

Shift current, a bulk photovoltaic effect, arises from nonlinear light–matter interaction in a noncentrosymmetric crystal under continuous wave illumination. Although it is a promising mechanism for photocurrent generation without p–n junctions, the short-circuit current (which is related to the power efficiency of a solar cell device) is usually low. It is therefore important to understand the physics of the phenomenon and find materials with strong shift current conductivity. We calculate the shift current conductivity including excitonic effects in a real material (monolayer GeS) from first principles. We show that electron–hole interactions can dramatically enhance and qualitatively change shift current in reduced-dimensional materials. Our results indicate low-dimensional materials are promising candidates for next-generation photovoltaic devices with high efficiencies.

Author contributions: S.G.L. designed research; Y.-H.C., D.Y.Q., and F.H.d.J. performed research; Y.-H.C., D.Y.Q., F.H.d.J., and S.G.L. analyzed the data; and Y.-H.C., D.Y.Q., F.H.d.J., and S.G.L. wrote the paper.

The authors declare no competing interest.

This article is a PNAS Direct Submission.

Published under the PNAS license.

[1]To whom correspondence may be addressed. Email: sglouie@berkeley.edu.

This article contains supporting information online at https://www.pnas.org/lookup/suppl/doi:10.1073/pnas.1906938118/-/DCSupplemental.

Published June 21, 2021.

Downloaded by guest on January 28, 2022

formalism on the Keldysh contour (19, 20). Our method allows us to consistently include many-electron interactions on both linear and nonlinear optical processes, which contrasts with the previous simplified first-principle study (11) that only includes the influence of excitonic effects on the profile of the light intensity as it penetrates a sample but still treats the intrinsic shift current response within an independent-particle picture. As we demonstrate below, the inclusion of excitonic effects on the shift current process is critically important since the shift current conductivity depends on virtual transitions between excitonic states and can dramatically alter the intrinsic nonlinear response when electron–hole interactions are strong. We illustrate the physics of many-electron interactions by computing the shift current coefficient tensor as a function of incident light frequency for a system that is atomically thin—a monolayer germanium sulfide (GeS). In addition to being an ab initio calculation of shift currents with contributions from subbandgap and above-bandgap frequency excitations in a real material, we show not only that self-energy and excitonic effects can enhance the total integrated shift current density by orders of magnitude, but also that many spectral features of the shift current coefficients are not even qualitatively captured by an independent particle (IP) picture. In particular, we show that, in monolayer GeS, excitonic effects strongly mix band states with different wavevector **k** in the Brillouin zone and thus yield a polarization anisotropy in the shift current that is much larger than what is found within an IP picture.

We start with the equation of motion for the interacting single-particle Green's function G on the Keldysh contour C,

$$\left[i\frac{d}{dt} - H(t)\right]G(t,t') = \delta(t,t') + \int_C \Sigma(t,\bar{t})G(\bar{t},t')d\bar{t}, \quad [1]$$

where $H = H_0 - e\mathbf{E}(t)\cdot\mathbf{r}$ is a mean-field Hamiltonian, which composes the electronic mean-field crystal Hamiltonian H_0 and an arbitrary time-dependent uniform external field **E** (which may be the field of the light); Σ is the electron self-energy operator; and G is the contour-ordered Green's function (*SI Appendix*). There is an equivalent adjoint equation for the time evolution over t', and we note that the $\boldsymbol{r}$ operator needs to be treated with care for a crystal. The self-energy is computed within the GW approximation (i.e., $\Sigma = iGW$), where W is the screened Coulomb potential (21). The solution to Eq. **1** provides the means to calculate various physical quantities, including the shift current.

One challenge in solving Eq. **1** is that the time evolution of G over t and t' has to be performed simultaneously. Following ref. 22, we decouple these equations by splitting the self-energy into that at equilibrium, $\Sigma[G_0]$, plus a correction term, $\delta\Sigma[G, G_0] = \Sigma[G] - \Sigma[G_0]$, where G_0 is the equilibrium Green's function with no external field. We evaluate $\Sigma[G_0]$ within the GW approximation (Σ^{GW}) and the correction $\delta\Sigma[G, G_0]$ within a static-screening scheme (i.e., the so-called static COHSEX) approximation (21). In the weak field limit, it has been shown that the resulting linearized equation of motion for G obtained this way yields an optical spectrum identical to the one from the ab initio GW-BSE approach computed with a statically screened electron–hole interaction kernel (22–24). Since this approach captures quasiparticle excitations given by the fully dynamical GW approximation at equilibrium and reproduces the optical response given by GW-BSE near equilibrium by neglecting memory effects, we refer to it as the time-dependent adiabatic GW (TD-aGW) approach in analogy to an adiabatic approximation to time-dependent density functional theory.

Within the TD-aGW approach, the equation of motion of G over t and t' can be rigorously rewritten (22) in terms of the interacting single-particle density matrix, ρ, evaluated in a quasiparticle basis: $\rho_{nm,\boldsymbol{k}} \equiv \langle n\boldsymbol{k}|\rho|m\boldsymbol{k}\rangle$,

$$i\hbar\frac{\partial}{\partial t}\rho_{nm,\boldsymbol{k}}(t) = \left[H_0(t) + \Sigma^{GW} + \delta\Sigma(t) - e\boldsymbol{E}\cdot\boldsymbol{r}, \rho\right]_{nm,\boldsymbol{k}}, \quad [2]$$

where n and m are band indices, and **k** is a **k** point in the Brillouin zone.

A challenge in dealing with Eq. **2** is that the position operator $\boldsymbol{r}$ is difficult to handle for extended states, although it can be formally separated into well-defined interband ($\boldsymbol{r}^{inter}$) and intraband ($\boldsymbol{r}^{intra}$) parts (25). Unlike in the case of linear optical processes in semiconductors at equilibrium and low temperatures for which only the interband part of $\boldsymbol{r}$ contributes, we also need to evaluate here the commutator $[\boldsymbol{r}^{intra}, \rho]_{nm\boldsymbol{k}}$, which involves the numerical derivative of the density matrix with respect to **k** and in turn involves an arbitrary **k**-dependent gauge. Here, we introduce the use of a locally smooth gauge using an idea similar to the covariant derivative (26, 27): We rotate wave functions at nearby **k** points so that the overlap of connected wave functions is Hermitian (26, 28). We find this local smooth gauge gives equivalent results to a global smooth gauge but at a negligible computational cost (*SI Appendix*). This technique is also an efficient alternative to replacing the general derivative by a summation of velocity and position matrices, as is commonly done in the field (4, 29).

Once the density matrix is known as a function of time through a real-time propagation of Eq. **2**, we may compute physical observables, such as the polarization and current density, by taking traces of the product of an appropriate operator with the density matrix. We compute the time-dependent current density as $\boldsymbol{J}(t) = Tr(\rho(t)\mathbf{v})$, where **v** is the velocity operator. To extract the shift current conductivity tensor, we evaluate the discrete Fourier components $\boldsymbol{J}_n$ from the current density computed under the coupling to a continuous wave monochromatic field (16) $\boldsymbol{E}(t) = \boldsymbol{E}_0 sin(\omega_E t)$. Responses at different harmonic frequencies can be computed by fitting to $\boldsymbol{J}(t) = \sum_{n=-S}^{S} \boldsymbol{J}_n e^{-i\omega_n t}$, where $\omega_n = n\omega_E$ with n as an integer, and S denotes the cutoff component of the Fourier series. The linear conductivity at finite frequencies, and hence the linear absorption coefficient, can be computed from $\boldsymbol{J}_1$. The shift current density is obtained from $\boldsymbol{J}_0$, and the second harmonic generation tensor can be computed from $\boldsymbol{J}_2$. More generally, higher harmonic responses may also be obtained from the fitting for Fourier components beyond $\boldsymbol{J}_2$.

Results and Discussion

We now present our results on excitonic effects on the shift current response tensor in monolayer GeS in the structure shown in Fig. 1 *A* and *B*, which was reported to have a relatively large shift current response in the IP approximation (30). We first verify the linear absorption spectrum calculated within our TD-aGW method against that from the ab initio GW-BSE approach, which was performed using the BerkeleyGW package (12, 21, 31). Density-functional theory calculations (as the starting mean field for the GW, GW-BSE, and TD-aGW calculations) were performed using the Quantum Espresso package (32) (see *SI Appendix* for computational details). The direct band gap for monolayer GeS, as computed from density-functional theory and GW, are 1.90 eV and 3.38 eV, respectively.

Fig. 1 depicts the computed linear absorption spectrum of monolayer GeS with normal incidence light polarized either along the zigzag (Fig. 1*D*) or armchair direction (Fig. 1*E*), defined as the x and y directions, respectively. The IP approximation with GW quasiparticle energies spectrum has an onset at 3.4 eV corresponding to the quasiparticle direct bandgap from our GW calculation. Comparing with the spectrum from the GW-BSE calculation, we find a binding energy of nearly 1.0 eV for the lowest energy optically active exciton, which agrees well with previous studies (33, 34).

We validate our TD-aGW method and code by comparing the linear optical absorption results from TD-aGW with those from the GW-BSE calculations. To obtain the linear responses at all frequencies, we apply an electric impulse at the beginning of the simulation and evaluate the time-dependent electric polarization $\boldsymbol{P}^e(t)$. The absorption spectrum $A(\omega)$ is computed from $\mathrm{Im}[P^{e,a}(\omega)/(\epsilon_0 E^b(\omega))]$, where a and b denote different components of the response tensor, relating to the direction of the induced electric polarization and incident electric field. Our TD-aGW results (with $a = b = y$) are shown in Fig. 1*E* by the blue dots and are virtually identical to the GW-BSE results.

In the time-propagation calculations, the contribution of light with a specific frequency ω to the DC shift current density along the a direction, denoted by $J_0^a(\omega)$, is given by (4)

$$J_0^a(\omega) = 2\sum_{bc}\sigma^{abc}(0;\omega,-\omega)E^b(\omega)E^c(-\omega), \quad [3]$$

where σ^{abc} is a second-order conductivity tensor, and a, b, and c are indices indicating the component of the shift current density and the polarization components of the incident light field (E^b and E^c) in Cartesian coordinates, respectively. The second-order conductivity tensor in principle can also be computed without performing an explicit time evolution of the density matrix, but it is quite conceptually and computationally involved for an interacting many-body system. Within the IP approximation, however, it can be obtained from the mean-field band structure and optical

Downloaded by guest on January 28, 2022

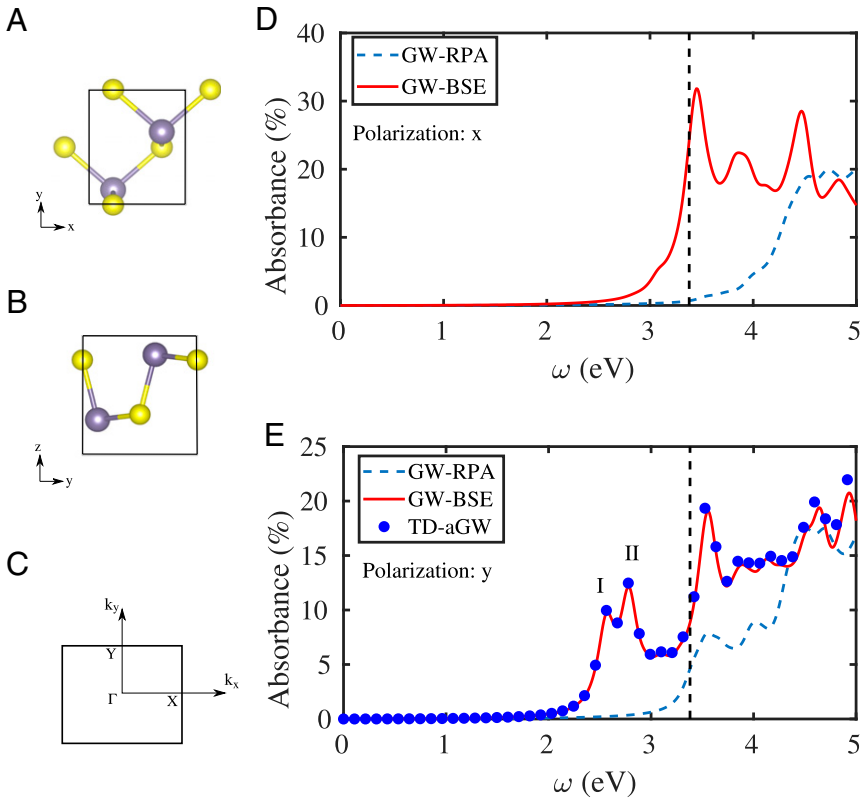

Fig. 1. Atomic model of a unit cell of monolayer GeS: (*A*) top view and (*B*) side view. (*C*) The Brillouin zone of monolayer GeS. Calculated linear absorption spectrum of monolayer GeS with *x*-polarized (*D*) and *y*-polarized (*E*) light at normal incidence: independent-particle approximation with GW quasiparticle energies (GW-RPA, blue dashed line), GW-BSE calculation (GW-BSE, red line), and TD-aGW calculation (TD-aGW, blue dots and only *y*-polarization results are shown). Both GW-BSE and TD-aGW results include electron–hole interaction (excitonic) effects, and all curves are generated with a Lorentzian broadening factor of 100 meV. Vertical dashed lines in *D* and *E* indicate the equilibrium bandgap. Peaks I and II in *E* correspond to absorption from formation of bound excitons within the bandgap.

interband transition matrix elements through the so-called sum-over-band formula in ref. 4. Within this formulation, it has been shown in recent studies (4, 35) that the shift current in the IP approximation depends on the absolute value of the interband transition matrix elements and the so-called shift vectors, which describe the change of the intracell position of Bloch wavefunction between the valence band and conduction band states involved in the optical transition.

In Fig. 2, we present two specific components of the shift current conductivity tensor as a function of photon frequency, with and without electron–hole coupling included in the calculations. The calculations were done on a 24 × 24 × 1 **k**-point mesh, and, for physical lifetime and convergence reasons, a dephasing factor that is equivalent to a spectral Lorentzian broadening of 100 meV was used in the time propagation. First, we see the striking results that there are large DCs generated by subbandgap photon frequencies at the exciton excitation energies. This remarkable phenomenon arises from many-body (electron–hole) interaction effects. Second, we see that at frequencies above the bandgap, around 3.5 eV, the largest peaks in the *yyy* component and in the *yxx* component are both enhanced by several orders of magnitude compared to the IP curves. This clearly illustrates the dramatic effects of excitonic effects on shift current generation, even inside the two-particle continuum. The enhancement factors here are spectacularly larger than those in the linear absorption, where excitonic effects at frequencies above the bandgap typically give an enhancement of only a factor of two. Upon including excitonic effects, the total shift current density integrated over the solar spectrum for the *yyy* component increases from 0.2 A/m^2 to 4.5 A/m^2, while that for the *yxx* component increases from 0.5 A/m^2 to 8.4 A/m^2 in monolayer GeS—roughly a 20-times enhancement compared with the noninteracting cases.

To get a better understanding of excitonic effects on the shift current responses, it is useful to formally look at an approximated "sum-over-exciton-state" formula derived from a linearized equation of motion (36). The approximated shift current tensor for a two-band model (with exciton states label by m and n) within this formalism is

$$\sigma^{abc}(0;\omega,-\omega)\sim\frac{-e^3}{m_e V_{\text{xtal}}}\sum_{m,n}\frac{P^a_m Q^b_{mn}\Omega^{c*}_n}{E_m(E_n-\hbar\omega-i\eta)}, \qquad [4]$$

where n and m are indices of the exciton states with a **k**-space envelope function of the nth exciton wavefunction given by ϕ^n_{cvk} and energy E_n (i.e., the many-body exciton state is expressed as $|\psi_m\rangle=\sum_{cvk}\phi^m_{cvk}|cvk\rangle$, with $|cvk\rangle$ denoting a free electron–hole interband excitation from a valence band v to a conduction band c at the wavevector $\boldsymbol{k}$), m_e is the electron mass, V_{xtal} is the crystal volume, $\boldsymbol{P}_m=\sum_k\phi^{(m)}_{cvk}\boldsymbol{p}_{vck}$ is an exciton transition matrix element to the mth exciton state, $\Omega_n=\sum_k\phi^n_{cvk}\boldsymbol{r}^{inter}_{cvk}$ is an exciton position matrix element, and $\boldsymbol{Q}_{mn}=i\sum_k\langle m|\partial_k|n\rangle$ is an interexciton position matrix element. (Note: We adopt the notation $\boldsymbol{r}_{nmk}=\langle nk|\boldsymbol{r}^{intra}|mk\rangle\delta_{nm}+\langle nk|\boldsymbol{r}^{inter}|mk\rangle(1-\delta_{nm})$ where $\mathbf{r}$ is the position operator.) In more succinct and physically transparent forms, $\boldsymbol{P}_m=\langle 0|\boldsymbol{p}|m\rangle$ and $\Omega_n=\langle 0|\boldsymbol{r}^{inter}|n\rangle$, which are the corresponding transition amplitudes between the ground state $|0\rangle$ and an exciton state $|m\rangle$ or $|n\rangle$.

Downloaded by guest on January 28, 2022

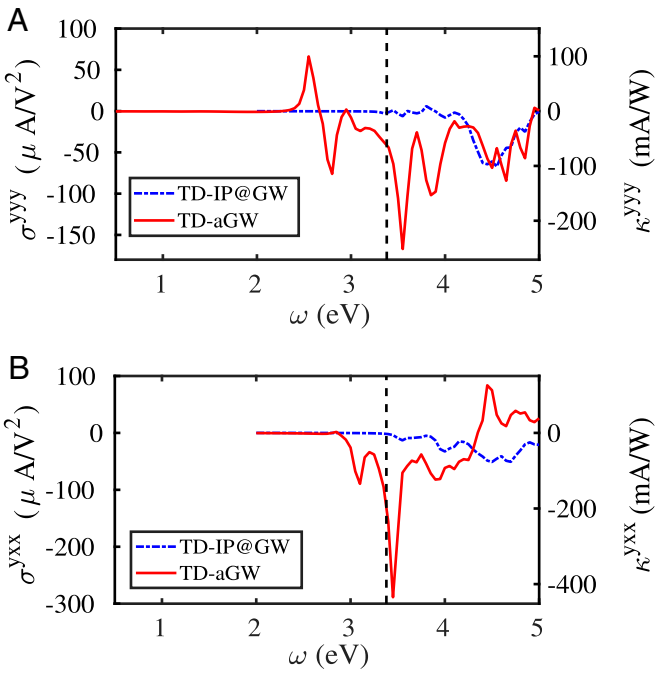

Fig. 2. Comparison of the shift current tensor components as function of frequency of monolayer GeS computed within a time-dependent independent-particle formalism with quasiparticle energies obtained from a GW calculation (blue dash-dotted line) and the TD-aGW (red solid line) method for (*A*) *yyy* and (*B*) *yxx* tensor components with the layer thickness taken to be 2.6 Å. The black dashed line indicates the position of the direct quasiparticle bandgap. The right vertical axis shows the corresponding response converted to units of photoresponsivity defined as the generated current per unit of incident radiant power.

From Eq. **4**, we see that the existence of bound excitons leads to an in-gap shift current response with resonant behavior at the exciton excitation energies, but in general it also involves other excitons with different energies. In practice, the shift current tensor in the subbandgap frequency regime will be further broadened due to inhomogeneous broadening and finite exciton lifetime effects, which are different from the traditional electron scattering time effects in the Drude conductivity. Moreover, the shift current is characteristically different from linear optical absorption. While the linear absorption spectrum is determined by $|\boldsymbol{e}\cdot\Omega_n|^2 = \left|\langle 0|\boldsymbol{e}\cdot\boldsymbol{r}^{inter}|n\rangle\right|^2$ summed over exciton states (where $\boldsymbol{e}$ is a polarization vector), the shift current involves the sum over the product of two distinct transition matrix elements from the ground state to two exciton states (m and n in Eq. **4** that may be different) multiplied by a third matrix element $\boldsymbol{Q}_{nm}$. Hence, the sharp exciton features in the shift current conductivity may exhibit more complex and strong optical anisotropy, depending on the incoming light polarization. Comparing Fig. 2*A* with Fig. 1*E*, we find that the first peak of the *yyy* tensor component of the shift current for monolayer GeS at 2.5 eV corresponds to the first peak in the linear absorption with *y*-polarized light at the same energy, and the second feature (a dip) in the response corresponds to the second peak in the linear absorption at 2.8 eV, which is due to an exciton in the valley along Γ–Y direction in the Brillouin zone. At other energies, the spectral features in the shift current conductivity tensor appear less sharp than the corresponding sharp excitonic peaks in the linear absorption spectrum.

We now elucidate the physics of the excitonic enhancement of the shift current in the two-particle (electron–hole) continuum. In the IP case, the spectral features in the shift current conductivity correlate with features in the shift vectors, $\boldsymbol{R}_{cv\boldsymbol{k}} \equiv \partial_{\boldsymbol{k}}\varphi_{cv\boldsymbol{k}} + \boldsymbol{r}_{cc\boldsymbol{k}} - \boldsymbol{r}_{vv\boldsymbol{k}}$, where the phases $\varphi_{cv\boldsymbol{k}}$ are defined as $\boldsymbol{r}_{cv\boldsymbol{k}} = |\boldsymbol{r}_{cv\boldsymbol{k}}|e^{-i\varphi_{cv\boldsymbol{k}}}$. From Eq. 4, in the excitonic case, we can define quantities analogous to the IP shift vectors using interexciton transition matrix elements $\boldsymbol{Q}_{nm}$. In particular, the diagonal elements $\boldsymbol{Q}_{nn}$ (we call the intraexciton terms) can be viewed as the exciton shift vector. However, our results show that the magnitudes of $\boldsymbol{Q}_{mn}$ do not significantly increase compared to the noninteracting case, since $\boldsymbol{Q}_{mn}$ can be regarded as a linear combination of the shift vectors (*SI Appendix*). Instead, the enhancement of the shift current conductivity comes primarily from an enhancement in the optical transition matrix elements P^a_m and Ω^c_n, particularly if excitons m and n are strongly bound in Eq. **4**. For example, in the case of extremely tightly bound excitons, the corresponding exciton envelope wavefunctions are extended over the Brillouin zone, resulting in $\left|\phi^m_{cv\boldsymbol{k}}\right| \sim 1/\sqrt{V_{\text{xtal}}}$, so $P^a_m\Omega^c_n \sim V_{\text{xtal}}$. Thus, a finite number of bound excitons give a finite contribution to the shift current conductivity instead of a vanishing contribution for a single vertical transition at a single **k** point in the IP case. This excitonic enhancement of the shift current conductivity due to an enhancement of the optical matrix elements is of analogous physical origin as in the case of linear optical absorption. Besides this effect, the additional nonlinear effects from interexciton couplings (i.e., the $m \neq n$ term in Eq. **4**) further contribute to the enhancement. We find, from a simple tight-binding model, the interexciton contribution is comparable to the intraexciton one (*SI Appendix*).

We now discuss how the presence of bound and strong resonant excitons affects the photovoltaic power efficiency of shift current materials. The power-conversion efficiency is related to both the short-circuit current and the open-circuit voltage. We have already shown that the current response (i.e., the short-circuit current) gets dramatically enhanced due to excitonic effects. For instance, comparing with the bulk ferroelectric material $BaTiO_3$, which has a shift current conductivity response of 5 μA/V^2 (5) in the same frequency range, monolayer GeS displays a response that is more than one order of magnitude larger and inside the electronic bandgap. It is of the same order of magnitude as the recently reported response in the Weyl semimetal tantalum arsenide (TaAs). The photoresponsivity κ (defined as the generated current per unit of incident radiant power; see κ on the right axis of Fig. 2) of monolayer GeS is also comparable to Si-based solar cells with reported $\kappa = 400$ mA/W (37). However, the total current density output by monolayer GeS when illuminated under the solar spectrum is at most only 4.5 A/m^2 (*SI Appendix*), roughly two orders of magnitude smaller than that in bulk Si. This smaller total current is due to the optical response of monolayer GeS not overlapping well with the solar spectrum, as it is restricted to a small range at high frequencies because of its large bandgap. We note that the photoresponsivity κ of Si here refers to a solar cell, which typically has an Si thickness of many microns to capture all the incoming photons, while the κ of a monolayer GeS device here is for an atomically thin material with a thickness of ∼0.2 nm and may be significantly increased by incorporating the GeS into a layered tandem device. Other materials with smaller bandgaps, such as GeSe, GeTe, SnS, SnSe, and SnTe, as suggested by previous first-principle IP calculations (30), might be better able to fully harness the solar spectrum using shift currents for photovoltaic applications.

While the short-circuit current depends on the shift current conductivity and not sensitively on the details of the sample, the same is not true for the open-circuit voltage. For instance, previous studies (38) argued that the open-circuit field E_{OC} for a shift current device would increase for samples with shorter carrier lifetimes (e.g., in disordered samples), as generated carriers cannot easily travel through the material. However, this previous conclusion assumes that the free carries present in the material are photoinduced and not coming from ionized defects. In a real material such as GeS, however, we expect that, even for clean

Downloaded by guest on January 28, 2022

samples, by having a bulk DC conductivity of $\sigma^{DC} \sim 10^{-2}(\Omega m)^{-1}$, the number of free carriers produced by ionizing defects will be of the order of 10^6 cm^{-2}, roughly four orders of magnitude larger than the interband photogenerated ones at steady state (*SI Appendix*). Therefore, the open-circuit field will clearly depend on the sample quality and defect concentration.

We can estimate the open-circuit field in the case of a finite concentration of shallow defects as $E_{oc} = J_{sc}/\sigma^{dc}$, where σ^{dc} is the sample's conventional DC conductivity. Using a current density of 4.5 A/m^2 for GeS under sunlight and a small bulk conductivity $10^{-2}(\Omega m)^{-1}$, we estimate the open-circuit field to be 450 V/m. From these, we see that the open-circuit voltage depends on the sample quality and the geometry of the device but not directly on the band gap of the material, which is in contrast to conventional solar cell devices based on traditional p–n junction. Consequently, it would be possible to take advantage of the excitonic enhancement of the short-circuit current and also obtain a large open-circuit voltage by minimizing the number of shallow impurity defects in shift current materials.

In summary, we have developed a theoretical framework and computer code to study nonlinear optical phenomena in real materials ab initio, including excitonic effects, and used the approach to calculate the shift current of monolayer GeS. We have shown that excitonic effects on the shift current give rise to DC current from optical excitations with in-gap frequencies as well as dramatic enhancement for above-gap frequencies. For monolayer GeS, the total current density integrated over the solar spectrum shows a 20-time enhancement due to exciton effects compared to the free electron–hole case. These findings add promise for using shift current for photovoltaic applications, allowing greater tunability and overlap with the solar spectrum. This work reveals the central importance of excitonic effects in shift current generation and opens pathways for designing highly efficient shift current devices from quasi–two-dimensional materials. It provides a perspective on the search for shift current materials for applications with efficiencies not bound by the Shockley-Queisser limit in traditional single p–n junction devices.

Data Availability. All study data are included in the article and/or *SI Appendix*.

ACKNOWLEDGMENTS. This work was supported by the Center for Computational Study of Excited State Phenomena in Energy Materials, which is funded by the US Department of Energy (DOE), Office of Science, Basic Energy Sciences, Materials Sciences and Engineering Division, under Contract No. DE-AC02-05CH11231, as part of the Computational Materials Sciences Program. Y.-H.C. thanks C. Attaccalite, T. Rangel, and T. Morimoto for helpful discussion. We acknowledge the use of computational resources at the National Energy Research Scientific Computing Center, a DOE Office of Science User Facility supported by the Office of Science of the US DOE under the above contract.

1. W. Kraut, R. von Baltz, Anomalous bulk photovoltaic effect in ferroelectrics: A quadratic response theory. *Phys. Rev. B Condens. Matter* **19**, 1548–1554 (1979).
2. B. I. Sturman, V. M. Fridkin, *The Photovoltaic and Photorefractive Effects in Noncentrosymmetric Materials* (Gordon and Breach Science Publishers, 1992).
3. C. Aversa, J. E. Sipe, Nonlinear optical susceptibilities of semiconductors: Results with a length-gauge analysis. *Phys. Rev. B Condens. Matter* **52**, 14636–14645 (1995).
4. J. E. Sipe, A. I. Shkrebtii, Second-order optical response in semiconductors. *Phys. Rev. B* **61**, 5337–5352 (2000).
5. L. Z. Tan *et al*., Shift current bulk photovoltaic effect in polar materials–hybrid and oxide perovskites and beyond. *npj Comput. Mater.* **2**, 16026 (2016).
6. A. M. Cook, B. M Fregoso, F. de Juan, S. Coh, J. E. Moore, Design principles for shift current photovoltaics. *Nat. Commun.* **8**, 14176 (2017).
7. M. Nakamura *et al*., Shift current photovoltaic effect in a ferroelectric charge-transfer complex. *Nat. Commun.* **8**, 281 (2017).
8. N. Ogawa, M. Sotome, Y. Kaneko, M. Ogino, Y. Tokura, Shift current in the ferroelectric semiconductor SbSI. *Phys. Rev. B* **96**, 241203 (2017).
9. J. Ibanez-Azpiroz, S. S. Tsirkin, I. Souza, *Ab initio* calculation of the shift photocurrent by Wannier interpolation. *Phys. Rev. B* **97**, 245143 (2018).
10. C. Wang *et al*., First-principles calculation of nonlinear optical responses by Wannier interpolation. *Phys. Rev. B* **96**, 115147 (2017).
11. R. Fei, L. Tan, A. Rappe, Shift current bulk photovoltaic effect influenced by quasiparticles and excitons. *Phys. Rev. B* **101**, 04510 (2020).
12. M. Rohlfing, S. G. Louie, Electron-hole excitations and optical spectra from first principles. *Phys. Rev. B Condens. Matter Mater. Phys.* **62**, 4927–4944 (2000).
13. T. Morimoto, N. Nagaosa, Topological aspects of nonlinear excitonic processes in noncentrosymmetric crystals. *Phys. Rev. B* **94**, 035117 (2016).
14. E. K. Chang, E. L. Shirley, Z. H. Levine, Excitonic effects on optical second-harmonic polarizabilities of semiconductors. *Phys. Rev. B* **65**, 035205 (2001).
15. R. Leitsmann, W. G. Schmidt, P. H. Hahn, F. Bechstedt, Second-harmonic polarizability including electron-hole attraction from band-structure theory. *Phys. Rev. B* **71**, 195209 (2005).
16. E. Luppi, H. Hbener, V. Vniard, *Ab initio* second-order nonlinear optics in solids: Second-harmonic generation spectroscopy from time-dependent density-functional theory. *Phys. Rev. B* **82**, 235201 (2010).
17. C. Attaccalite, M. Grüning, Nonlinear optics from an *ab initio* approach by means of the dynamical berry phase: Application to second- and third-harmonic generation in semiconductors. *Phys. Rev. B Condens. Matter Mater. Phys.* **88**, 235113 (2013).
18. M. Grüning, C. Attaccalite, Second harmonic generation in h-BN and MoS_2 monolayers: Role of electron-hole interaction. *Phys. Rev. B Condens. Matter Mater. Phys.* **89**, 081102 (2014).
19. L. V. Keldysh, Diagram technique for nonequilibrium processes. *Sov. Phys. JETP* **20**, 1018 (1965).
20. L. P. Kadanoff, G. Baym, *Quantum Statistical Mechanics* (W.A. Benjamin, 1962).
21. M. S. Hybertsen, S. G. Louie, Electron correlation in semiconductors and insulators: Band gaps and quasiparticle energies. *Phys. Rev. B Condens. Matter* **34**, 5390–5413 (1986).
22. C. Attaccalite, M. Grüning, A. Marini, Real-time approach to the optical properties of solids and nanostructures: Time-dependent Bethe-Salpeter equation. *Phys. Rev. B Condens. Matter Mater. Phys.* **84**, 245110 (2011).
23. D. Rocca, D. Lu, G. Galli, Ab initio calculations of optical absorption spectra: Solution of the Bethe-Salpeter equation within density matrix perturbation theory. *J. Chem. Phys.* **133**, 164109 (2010).
24. E. Rabani, R. Baer, D. Neuhauser, Time-dependent stochastic Bethe-Salpeter approach. *Phys. Rev. B* **91**, 235302 (2015).
25. E. I. Blount, Formalisms of band theory. *Solid State Phys.* **13**, 305–373 (1962).
26. I. Souza, J. Íñiguez, D. Vanderbilt, Dynamics of berry-phase polarization in time-dependent electric fields. *Phys. Rev. B Condens. Matter Mater. Phys.* **69**, 085106 (2004).
27. K. S. Virk, J. E. Sipe, Semiconductor optics in length gauge: A general numerical approach. *Phys. Rev. B Condens. Matter Mater. Phys.* **76**, 035213 (2007).
28. N. Marzari, D. Vanderbilt, Maximally localized generalized wannier functions for composite energy bands. *Phys. Rev. B Condens. Matter* **56**, 12847–12865 (1997).
29. J. L. Cabellos, B. S. Mendoza, M. A. Escobar, F. Nastos, J. E. Sipe, Effects of nonlocality on second-harmonic generation in bulk semiconductors. *Phys. Rev. B Condens. Matter Mater. Phys.* **80**, 155205 (2009).
30. T. Rangel *et al*., Large bulk photovoltaic effect and spontaneous polarization of single-layer monochalcogenides. *Phys. Rev. Lett.* **119**, 067402 (2017).
31. J. Deslippe *et al*., BerkeleyGW: A massively parallel computer package for the calculation of the quasiparticle and optical properties of materials and nanostructures. *Comput. Phys. Commun.* **183**, 1269–1289 (2012).
32. P. Giannozzi *et al*., Quantum espresso: A modular and open-source software project for quantum simulations of materials. *J. Phys. Condens. Matter* **21**, 395502 (2009).
33. L. C. Gomes, P. E. Trevisanutto, A. Carvalho, A. S. Rodin, A. H. Castro Neto, Strongly bound mott-wannier excitons in GeS and GeSe monolayers. *Phys. Rev. B* **94**, 155428 (2016).
34. L. Xu, M. Yang, S. J. Wang, Y. P. Feng, Electronic and optical properties of the monolayer group-IV monochalcogenides MX (M = Ge, Sn; X = S, Se, Te). *Phys. Rev. B* **95**, 235434 (2017).
35. T. Morimoto, N. Nagaosa, Topological nature of nonlinear optical effects in solids. *Sci. Adv.* **2**, e1501524 (2016).
36. T. G. Pedersen, Intraband effects in excitonic second-harmonic generation. *Phys. Rev. B Condens. Matter Mater. Phys.* **92**, 235432 (2015).
37. G. B. Osterhoudt *et al*., Colossal mid-infrared bulk photovoltaic effect in a type-I Weyl semimetal. *Nat. Mater.* **10**, 1038 (2019).
38. T. Morimoto, M. Nakamura, M. Kawasaki, N. Nagaosa, Current-voltage characteristic and shot noise of shift current photovoltaics. *Phys. Rev. Lett.* **121**, 267401 (2018).

Downloaded by guest on January 28, 2022